pH-dependent Growth of Atomic Pd Layers on Trisoctahedral Gold Nanoparticles to Realize Enhanced Performance in Electrocatalysis and Chemical Catalysis

Yahui Song,[a] Chensheng Xiang,[d] Cuixia Bi,[a] Chenshuo Wu,[a] Hongpeng He,[a] Wei Du,[b] Lihui Huang,[c] He Tian[*,d] and Haibing Xia[*,a]

[a]State Key Laboratory of Crystal Materials, Shandong University, Jinan, 250100, P. R. China;

[b]School of Environment and Material Engineering, Yantai University, Yantai 264005, Shandong, China;

[c]School of Environmental Science and Engineering, Shandong University, Jinan, 250100, P. R. China.

[d]Center of Electron Microscope, State Key Laboratory of Silicon Materials, School of Materials Science and Engineering, Zhejiang University, Hangzhou, 310027, China.

Figure S1. TEM images of TOH Au@Pd$_{island}$ NPs prepared in the aqueous CTAC solution with a pH of 7.5. The molar ratio of Pd precursor to TOH Au NPs are 1:48 and 1:16 in (A) and (B), respectively.
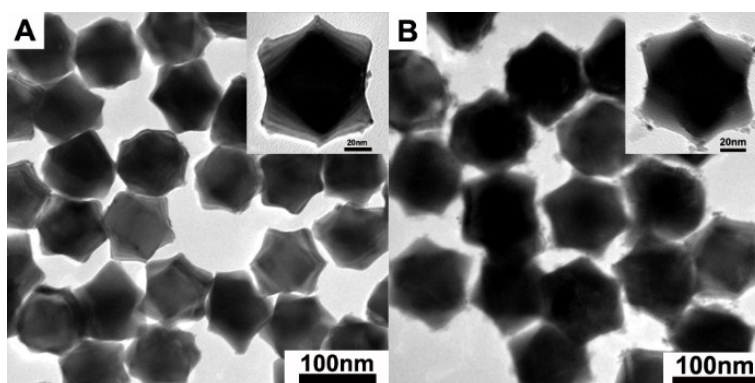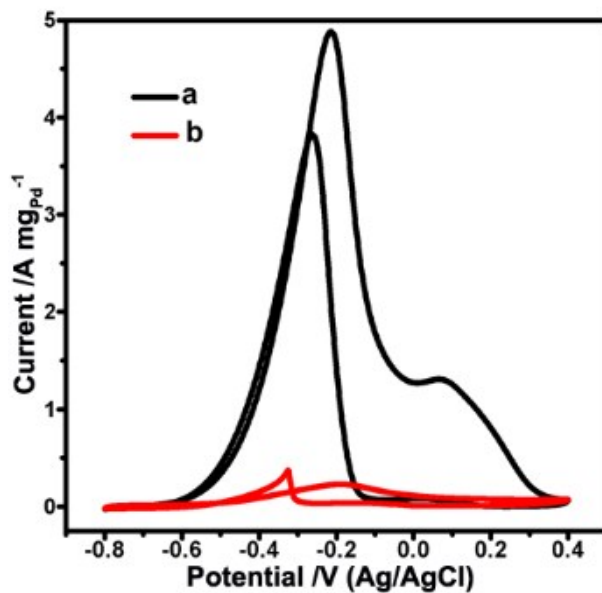
Figure S2. CV curves of GCEs modified with TOH Au@Pd$_{island}$ NPs (a, black curve, the sample shown in Figure S1A) and commercial Pd/C catalysts (b, red curve), respectively, measured in 0.5 M KOH solution in the presence of 0.5 M ethanol. The scan rate is 20 mV s^{-1}. The currents are normalized by the Pd mass loaded.

The electrocatalytic performance on ethanol oxidation of the resulting TOH Au@Pd$_{island}$ NPs (4.9 A mg$_{Pd}^{-1}$) is only 24.5-fold better than that of the commercial Pd/C catalysts (0.2 A mg$_{Pd}^{-1}$).

Figure S3. Representative SERS spectra of 4-ATP molecules (1×10^{-4} M) adsorbed on the aggregates of TOH Au NPs (a, black curve) and TOH Au@Pd$_{island}$ NPs (b, red curve, the sample shown in Figure S1A). The excitation laser wavelength for Raman measurements is 633 nm. The acquisition time is 10 s.
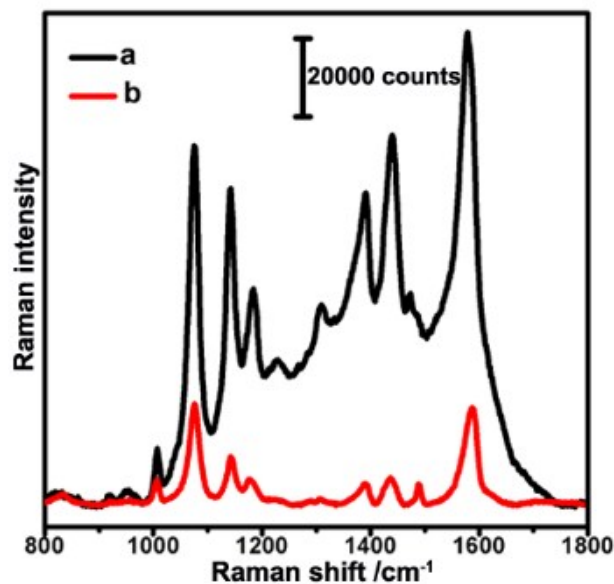
The TOH Au@Pd$_{island}$ NPs exhibit much lower SERS signals than the TOH Au NPs possibly because the Pd particles aggregated on the sharp extremities of the TOH Au NPs and thus impact these hot-spots for SERS performance (Figure S3).

Figure S4. Representative TEM images of TOH Au@Pd$_{3L}$ NPs with Pd shell of 4 atomic Pd layer prepared in the aqueous CTAC solution with a pH of 3.3.
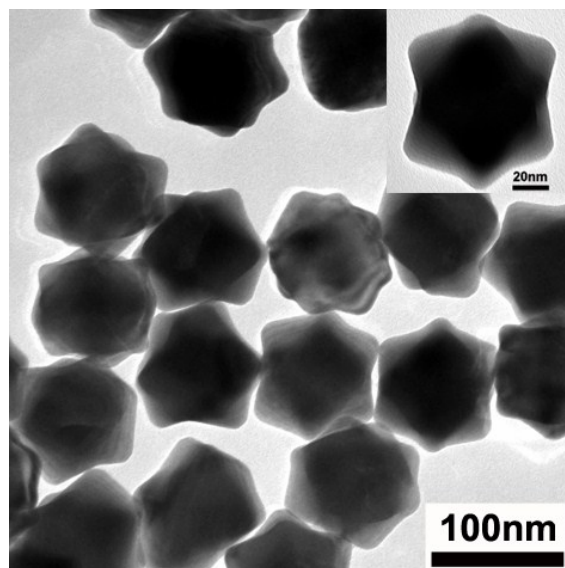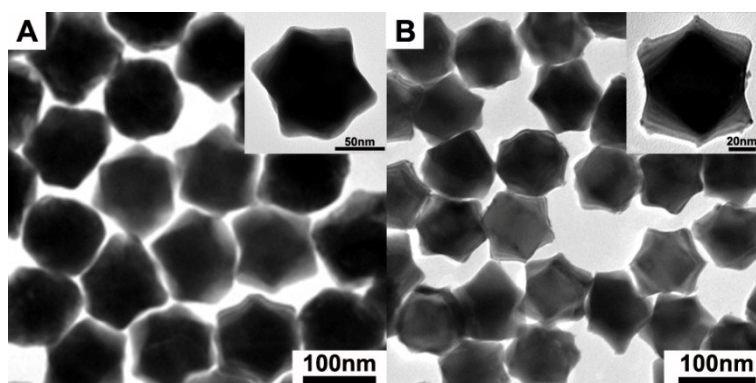
Figure S5. Typical TEM images of TOH Au@Pd NPs prepared in the aqueous CTAC solution with different pH values: (A) with pH values of from 2.2 to 5.5, and (B) with a pH value of 7.5. The amount of Pd precursor used is all the same.

It is known that the electrocatalytic performance of the resulting Au@Pd NPs are determined by the state of Pd shell. In addition, the state of Pd shells would can be significantly impacted by the pH values of the growth solution. Thus, a series of TOH Au@Pd NPs were prepared at different pH values of the aqueous CTAC solution (Figure S5) and their electrocatalytic performance were also characterized (Figure S6 and Table S1). On the basis of their TEM images, the difference among TOH Au@Pd NPs prepared at pH values from 2.2 to 5.5 cannot be distinguished as they all bear smooth surfaces (Figure S5A), while there are some small particles formed on the surfaces of TOH Au@Pd NPs prepared at pH value of 7.5 (Figure S5B).

Their electrocatalytic performances on ethanol oxidation were further investigated and compared to select the optimal pH value for synthesis of Au@Pd NPs (Figure S6). It was found that mass activities and specific activities both show a "volcano-type" dependence on the pH value of the aqueous CTAC solution. The TOH Au@Pd NPs prepared in the aqueous CTAC solution with a pH of 3.3 exhibit the optimal electrocatalytic performance. Therefore, the optimal pH value of the aqueous CTAC solution used for the growth of Pd shell on the surface of Au NPs is 3.3.

Figure S6. CV curves (A and B) of GCEs modified with TOH Au@Pd NPs prepared in the aqueous CTAC solution with different pH values: 2.2 (a, red curve), 3.1 (b, black curve), 3.3 (c, blue curve), 3.7 (d, dark cyan curve), 3.9 (e, magenta curve), 4.3 (f, dark yellow curve), 5.5 (g, navy curve), and 7.5 (h, wine curve), measured in 0.5 M KOH aqueous solution in the presence of 0.5 M ethanol. The currents of (A) and (B) were normalized by the Pd mass loaded on GCE and the ECSA values, respectively. The scan rates of (A and B) both are 20 mV s^{-1}. The amount of Pd precursor used is all the same.
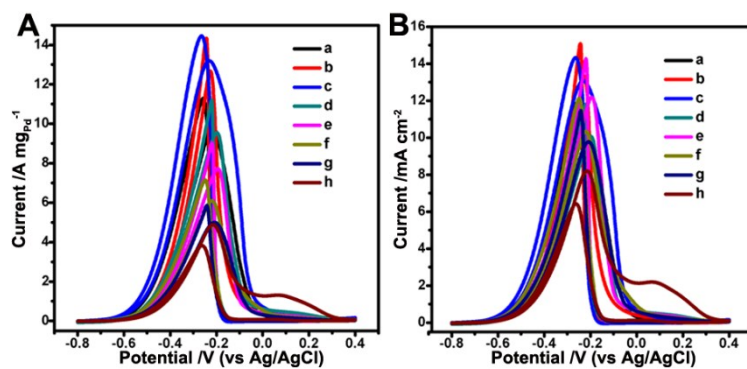
Figure S7. The geometrical model (a) of a single TOH NP viewed along the <110> direction. TEM images (b) of the TOH Au NP bounded by {331} planes, viewed along the <110> direction. The atomic models (c) of the {331} planes projected from the [110] zone axis. HRTEM images (d) of edge-on facets viewed along the <110> direction showing the {331} facets. The centers of surface atoms are indicated by red dots.
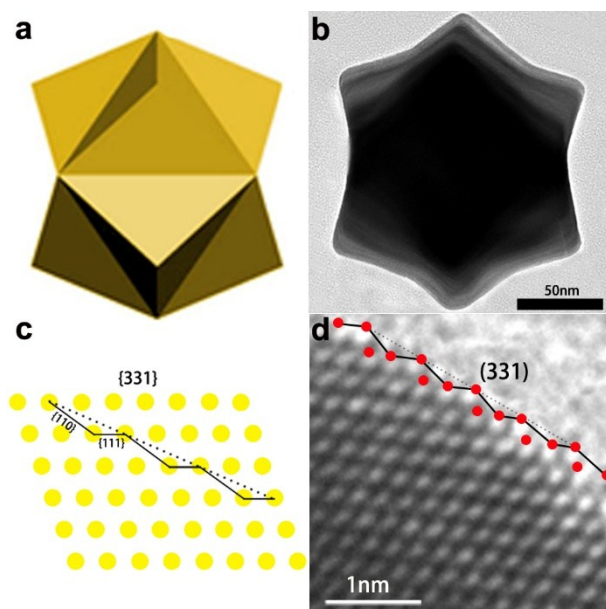
Figure S8. CV curves of pure TOH Au cores (black curve) and the TOH Au@Pd$_{0.75L}$ NPs with not completely covered by Pd shell (red curve) and the TOH Au@Pd$_{1L}$ NPs (blue curve), tested in 0.50 M N$_2$-saturated KOH aqueous solution at room temperature.
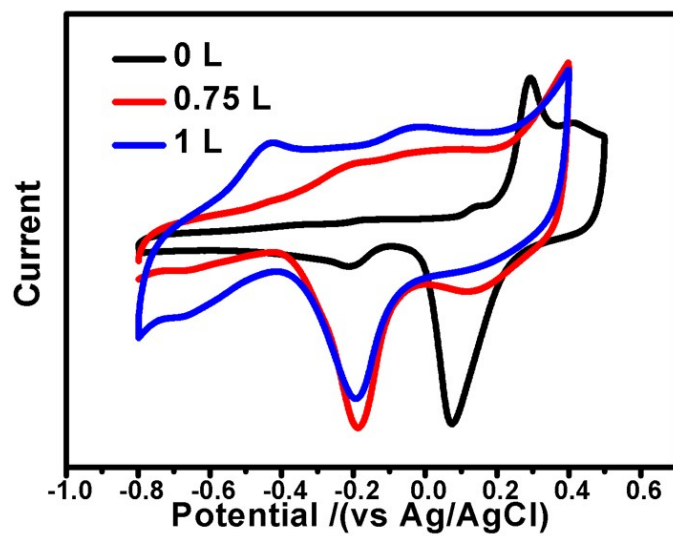
Figure S9. Representative TEM images of TOH Au@Pd$_{12L}$ NPs with Pd shell of 12 atomic Pd layer prepared in the aqueous CTAC solution with a pH of 3.3.
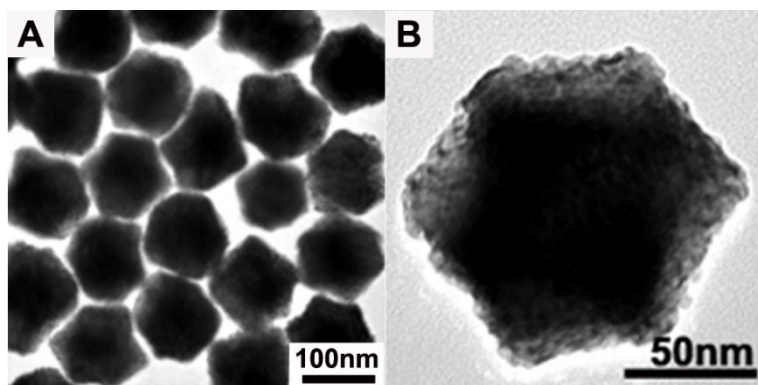
Figure S10. Schematic depiction of three typical growth modes of Pd on the surface of TOH Au NPs with increasing Pd layer (L): (a) Volmer-Weber growth (V-W mode, island growth), (b) Stranski-Krastanow growth (S–K mode, layer-plus-island growth), and (c) Frank-van der Merwe growth (F-M mode, layer-by-layer growth).
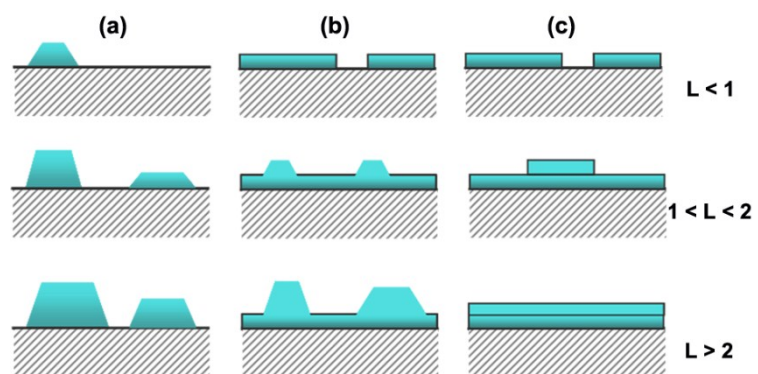
Figure S11. CV curves of GCEs modified with the corresponding TOH Au@Pd$_{island}$ NPs prepared in the growth solution containing CTAC with a pH value of 7.5 in 0.5 M H$_2$SO$_4$ media. The amounts of Pd used for synthesis of the corresponding TOH Au@Pd$_{island}$ NPs are the same as those used for synthesis of the corresponding TOH Au@Pd$_{nL}$ NPs (in Figure 2): 0 L (a, black curve), 0.25 L (b, red curve), 0.38 L (c, blue curve), 0.75 L (d, dark cyan curve), and 1.5 L (e, magenta curve), respectively. The scan rate is 50 mV s^{-1}.
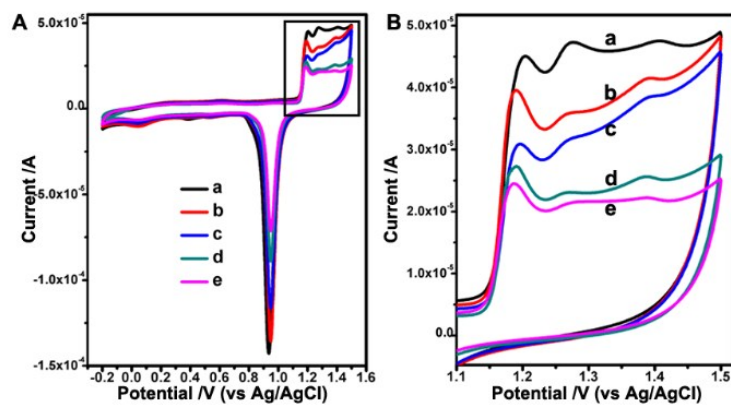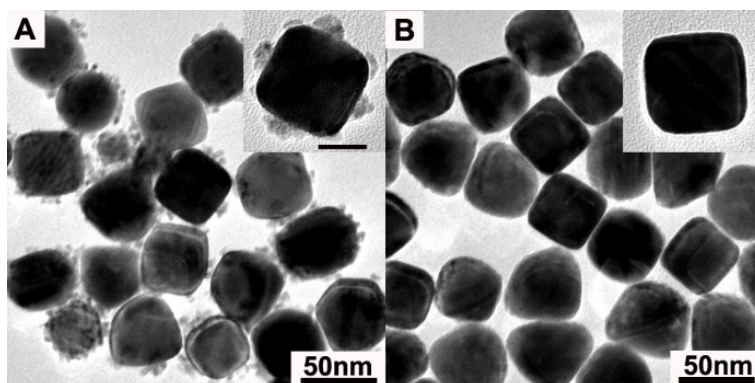
Figure S12. TEM images of cubic Au@Pd$_{island}$ NPs (A) and cubic Au@Pd$_{3L}$ NPs (B) prepared in aqueous CTAC solution with a pH of 7.5 and 3.3, respectively.

Cubic Au@Pd NPs (Figure S12) and spherical Au@Pd NPs (Figure S13) were then prepared in the aqueous CTAC solution with pH values of 7.5 and 3.3, respectively. When the pH value of the aqueous CTAC solution was 7.5, numerous small Pd NPs chaotically deposited on the surfaces of cubic Au NPs (Figure S12A) and spherical Au@Pd NPs (Figure S13A), respectively. However, when the pH value of the aqueous CTAC solution was adjusted to 3.3, cubic Au@Pd NPs (Figure S12B) and spherical Au@Pd NPs (Figure S13B) both show smooth surfaces and there are no nanoscale surface protrusions observed on their surfaces, indicating the epitaxy growth of Pd onto their surfaces. Thus, the growth mode of Pd onto Au NPs in the presence of CTAC can be regulated by pH value of the growth solution.

Figure S13. TEM images of the spherical Au@Pd$_{island}$ NPs (A) and spherical Au@Pd$_{3L}$ NPs (B) prepared in growth solution with a pH of 7.5 and 3.3, respectively.
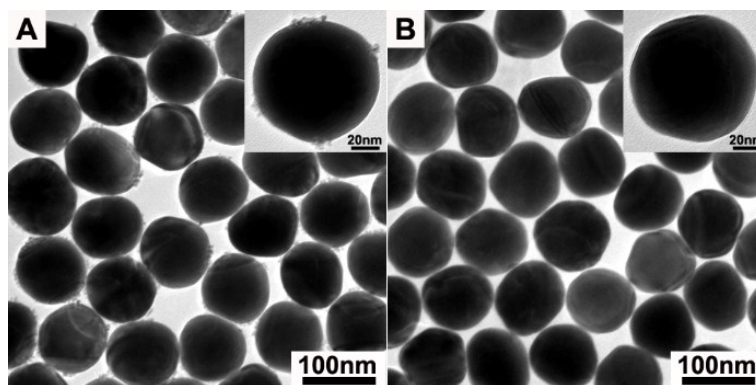
Figure S14. CV curves (A to C) of GCEs modified with TOH Au@Pd$_{nL}$ NPs with different Pd atomic layers: 3 L (a, black curve), 2 L (b, red curve), 1.5 L (c, blue curve), 1.2 L (d, cyan curve), 1 L (e, magenta curve), and 0.75 L (f, yellow curve) , respectively, which were measured in 0.5 M KOH aqueous solution in the absence (A) and presence (B and C) of 0.5 M ethanol. The currents of (A and B) and (C) were normalized by the Pd mass loaded on GCE and the ECSA values, respectively. The scan rates of (A) and (B and C) are 50 mV s^{-1} and 20 mV s^{-1}, respectively.   These TOH Au@Pd$_{nL}$ NPs were prepared in aqueous CTAC solution with a pH of 3.3.
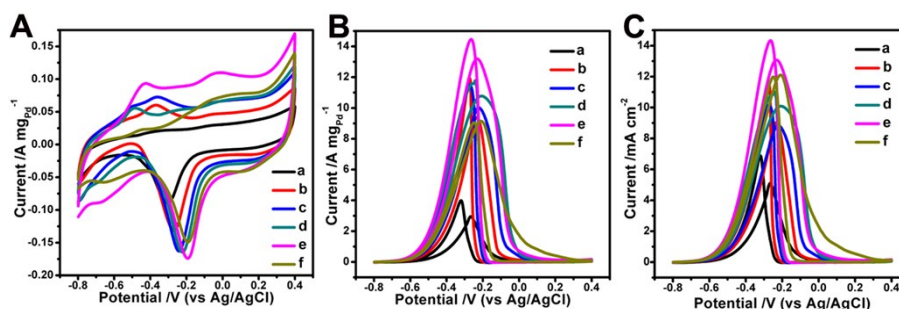
To obtain TOH Au@Pd$_{nL}$ NPs with optimal electrocatalytic performance, as-prepared TOH Au@Pd$_{nL}$ NPs with different Pd atomic layers toward ethanol oxidation were investigated. The electrochemical active surface area (ECSA) can be determined using the surface charge associated with the reduction of their oxide in the CV curves in an alkaline medium. The peaks around -0.2 V during the negative sweep are associated with the reduction of Pd oxide species on the surfaces of NPs. The charge associated with the reduction of oxide species for pure Pd is 430 μC cm^{-2}. Their ECSA values are calculated to be 57.9, 104.0, 113.2, 106.9, 100.9, and 75.5 m^2 g^{-1}, respectively(Figure S14A and Table S2). Moreover, the surfaces of the resulting NPs can be exclusively covered by Pd when the number of Pd atomic layers is equal or higher than 1, as no noticeable fraction of Au is present on the surfaces of NPs on the basis of results of CV curves[1,2] (Figure S14A). Figure S14B depicts the mass activities of TOH Au@Pd$_{nL}$ NPs with different numbers of Pd atomic layers were 2.9, 9.3, 10.1, 10.8, 13.2, and 9.2 A mg^{-1}, respectively. Their specific activities are 5.1, 9.0, 8.9, 10.1, 13.1, and 12.1 mA cm^{-2}, respectively (Figure S14C and Table S2), normalized by their ECSA values. It was found that mass activities and specific activities both follows a volcano trend with respect to their number of Pd atomic layers.

In a word, the electrocatalytic performance of TOH Au@Pd$_{1L}$ NPs was optimal considering mass- and specific activities as a whole.

Figure S15. HAADF-STEM-EDS mapping images (A) and HAADF-STEM image with cross-sectional compositional line profile (B) of one single TOH Au@Pd$_{12L}$ NP.

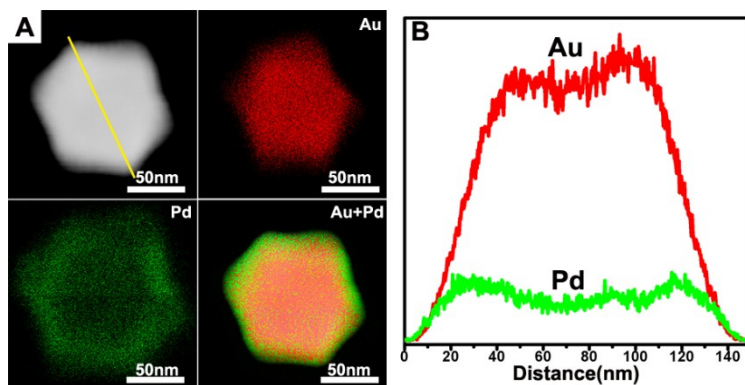**Figure S16.** XRD pattern of as-prepared TOH Au@Pd$_{1L}$ NPs prepared in the aqueous CTAC solution with a pH value of 3.3.
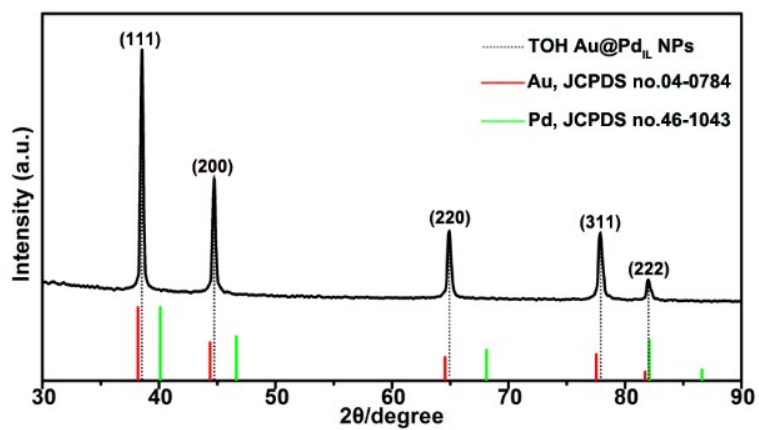
Figure S17. XRD pattern of as-prepared TOH Au@Pd$_{12L}$ NPs prepared in the aqueous CTAC solution with a pH value of 3.3.
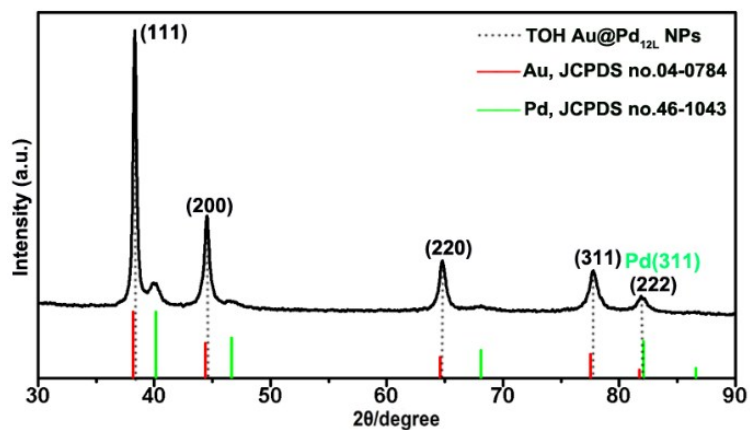
Figure S18. XPS spectra of the Pd 3d signals of pure Pd NPs (A) and TOH Au@Pd$_{1L}$ NPs prepared in the aqueous CTAC solution with a pH value of 3.3 (B).
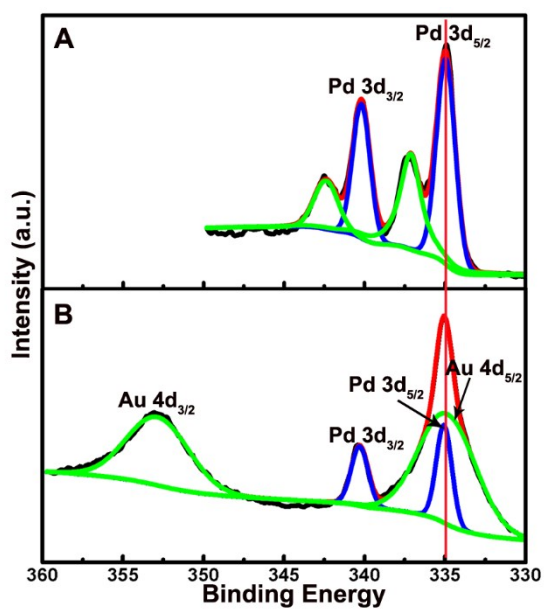
Figure S19. XPS spectra of the Au 4f signals of TOH Au NPs (A) and TOH Au@Pd$_{1L}$ NPs prepared in the aqueous CTAC solution with a pH value of 3.3 (B).
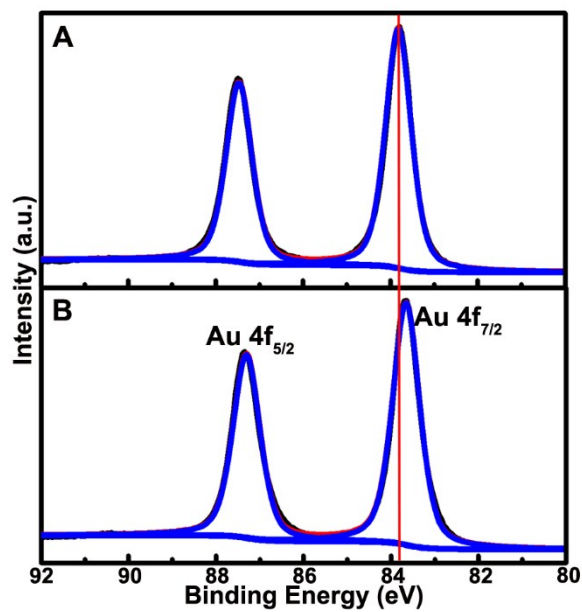
Figure S20. CV curves (A, B and C) of the GCE modified with TOH Au@Pd$_{1L}$ NPs (a, black curve), cubic Au@Pd$_{1L}$ NPs (b, red curve), and spherical Au@Pd$_{1L}$ NPs (c, blue curve), measured in 0.5 M KOH solution in the absence (A) and presence (B and C) of 0.5 M ethanol. The scan rates of (A) and (B and C) are 50 mV s^{-1} and 20 mV s^{-1}, respectively. The currents of (A and B) and (C) were normalized by the Pd mass loaded on GCE and the ECSA values, respectively. These differently-shaped Au@Pd$_{1L}$ NPs were prepared in aqueous CTAC solution with a pH of 3.3.
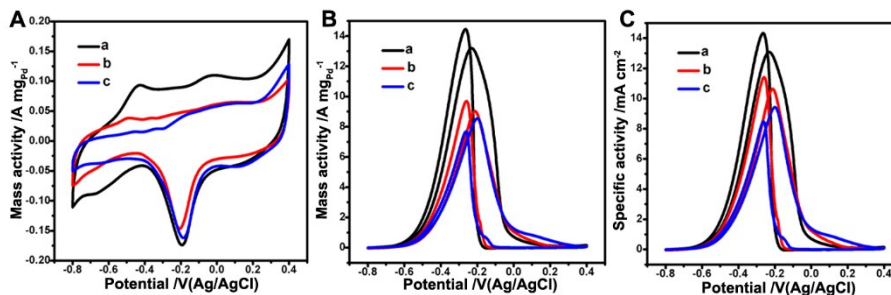
The electrocatalytic activities of as-prepared TOH Au@Pd$_{1L}$ NPs, cubic Au@Pd$_{1L}$ NPs, and spherical Au@Pd$_{1L}$ NPs toward ethanol oxidation were investigated (Figure S20). The ECSA values of TOH Au@Pd$_{1L}$ NPs, cubic Au@Pd$_{1L}$ NPs, and spherical Au@Pd$_{1L}$ NPs are calculated to be 100.9, 84.9, and 90.7 m^2 g^{-1}, respectively (Figure S20A and Table S6); and TOH Au@Pd$_{1L}$ NPs have the highest ECSA value. Figure S20B depicts the mass activities of TOH Au@Pd$_{1L}$ NPs, cubic Au@Pd$_{1L}$ NPs, and spherical Au@Pd$_{1L}$ NPs, which are 13.2, 9.0, and 8.6 A mg$_{Pd}^{-1}$, respectively (Figure S20B and Table S6). Their specific activities are 13.1, 10.6, and 9.4 mA cm^{-2}, respectively (Figure S20C and Table S6). All of results demonstrate that TOH Au@Pd$_{1L}$ NPs (100.9 m^2 g^{-1}, 13.2 A mg$_{Pd}^{-1}$, and 13.1 mA cm^{-2}) show the best electrocatalytic performance for ethanol oxidation.

Figure S21. CV curves (A to C) of GCEs modified with TOH Au@Pd$_{island}$ NPs (a, black curve), cubic Au@Pd$_{island}$ NPs (b, red curve), spherical Au@Pd$_{island}$ NPs (c, blue curve) measured in 0.5 M KOH aqueous solution in the absence (A) and presence(B and C) of 0.5 M ethanol. The currents of (A and B) and (C) were normalized by the Pd mass loaded on GCE and the ECSA values, respectively. The scan rates of (A) and (B and C) are 50 mV s^{-1} and 20 mV s^{-1}, respectively. These differently-shaped Au@Pd$_{island}$ NPs were prepared in aqueous CTAC solution with a pH of 7.5 and other reaction conditions are same to those of the corresponding Au@Pd$_{1L}$ NPs.
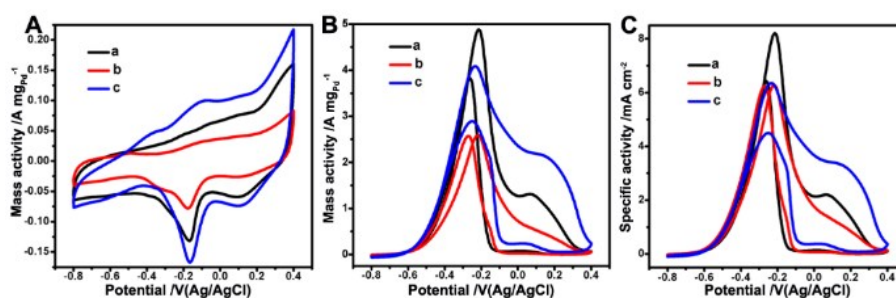
The electrocatalytic activities of TOH Au@Pd$_{island}$ NPs, cubic Au@Pd$_{island}$ NPs, and spherical Au@Pd$_{island}$ NPs are also investigated (Figure S21 and Table S6). Accordingly, the ECSA values of TOH Au@Pd$_{island}$ NPs, cubic Au@Pd$_{island}$ NPs and spherical Au@Pd$_{island}$ NPs are calculated to be 49.6, 41.2, and 64.3 m^2 g^{-1}, respectively (Figure S21A and Table S6); the mass activities of TOH Au@Pd$_{island}$ NPs, cubic Au@Pd$_{island}$ NPs, and spherical Au@Pd$_{island}$ NPs, are 4.9, 2.6, and 4.1 A mg$_{Pd}$$^{-1}$, respectively (Figure S21B and Table S6); and their specific activities are 8.2, 6.3, and 6.4 mA cm^{-2}, respectively (Figure S21C and Table S6). In comparison with those of their corresponding Au@Pd$_{1L}$ NPs, ECSA values, mass and specific activities of TOH Au@Pd$_{island}$ NPs, cubic Au@Pd$_{island}$ NPs, and spherical Au@Pd$_{island}$ NPs all drastically decreased (Figure S20, S21 and Table S6). These results indicate that the core-shell Au@Pd NPs with epitaxy growth of Pd shell can significantly improve the electrocatalytic performance, compared with those with island growth of Pd shell.

Figure S22. UV-vis spectra of the reduction of 4-NP by NaBH$_4$ at different time intervals since the catalytic reaction started in the presence of TOH Au NPs (A) and TOH Au@Pd$_{island}$ NPs (B), and TOH Au@Pd$_{1L}$ NPs (C). TOH Au NPs (A) and TOH Au@Pd$_{island}$ NPs (B), and TOH Au@Pd$_{1L}$ NPs (C) were prepared in aqueous CTAC solution with a pH of 7.5 (B) and 3.3 (C), respectively.
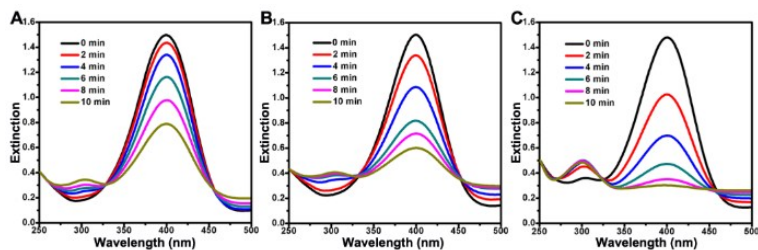
This reaction also can be easily monitored by UV-visible spectroscopy because 4-nitrophenolate ions and 4-aminophenol (4-AP) both display strong absorption bands centered at 400 and 300 nm, respectively. Figure. S22 shows the absorption spectra of the reduction of 4-NP by NaBH$_4$ as a function of reaction time when the reduction were catalyzed by TOH Au NPs (A), TOH Au@Pd$_{island}$ NPs (B), and TOH Au@Pd$_{1L}$ NPs (C), respectively.

Figure S23. Plot of $\ln(A/A_0)$ against the reaction time of the reduction of 4-NP by $NaBH_4$ in the presence of TOH Au NPs (black curve), TOH Au@Pd$_{island}$ NPs (red curve), and TOH Au@Pd$_{1L}$ NPs (blue curve), respectively.
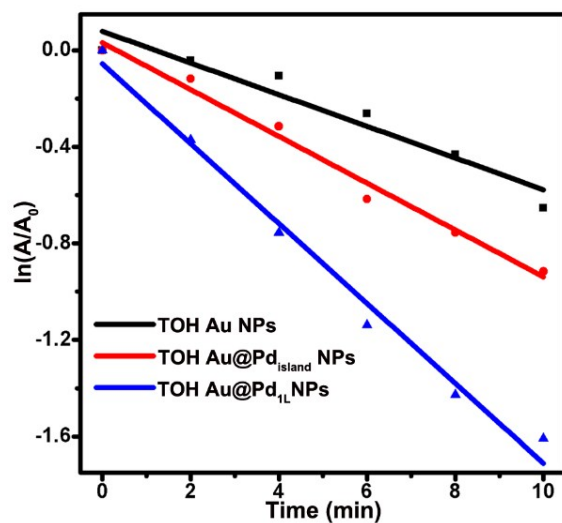
To compare the catalytic activities of the TOH Au NPs, TOH Au@Pd$_{island}$ NPs, and TOH Au@Pd$_{1L}$ NPs, $\ln(A/A_0)$ is plotted as a function of reaction time (Figure S23), where A and A_0 are the relative concentrations of 4-NP at time $t = t$ and $t = 0$, respectively.

Figure S24. The normal Raman spectra of 4-NTP and 4-ATP molecules in powder.

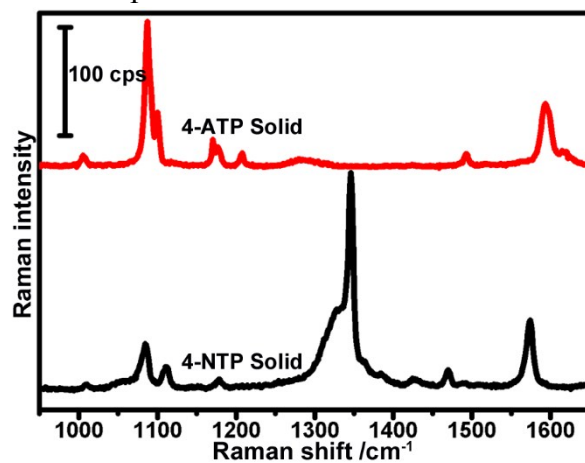**Table S1.** Summarized data of mass activities and specific activities of TOH Au@Pd NPs prepared in the aqueous CTAC solution with different pH values.

pH	Mass activity [A mg_{Pd}^{-1}]	Specific activity [mA cm^{-2}]
2.2	9.9	10.4
3.1	12.7	13.3
3.3	13.2	13.1
3.7	9.5	10.1
3.9	7.7	12.2
4.3	6.1	10.4
5.5	5.0	9.8
7.5	4.9	8.2

Table S2. Summarized data of ECSA values, mass activities, and specific activities of TOH Au@Pd$_{nL}$ NPs with different Pd atomic layers.

Sample	Number of Pd atomic layers (n)	ECSA [m^2 g$_{Pd}^{-1}$]	Mass activity [A mg$_{Pd}^{-1}$]	Specific activity [mA cm^{-2}]
TOH Au@Pd$_{3L}$ NPs	3	57.9	2.9	5.1
TOH Au@Pd$_{2L}$ NPs	2	104.0	9.3	9.0
TOH Au@Pd$_{1.5L}$ NPs	1.5	113.2	10.1	8.9
TOH Au@Pd$_{1.2L}$ NPs	1.2	106.9	10.8	10.1
TOH Au@Pd$_{1L}$ NPs	1	100.9	13.2	13.1
TOH Au@Pd$_{0.75L}$ NPs	0.75	75.5	9.2	12.1

Table S3. Summary of the total compositions of TOH Au@Pd$_{1L}$ NPs by ICP-MS.

Sample	Au(%)	Pd(%)
TOH Au@Pd$_{1L}$ NPs	98.44	1.56

Table S4. XPS shifts of the Pd 3d signals of pure Pd NPs and TOH Au@Pd$_{1L}$ NPs prepared in aqueous CTAC solution with a pH of 3.3.

Sample	Pd 3d$_{5/2}$ peak (eV)	Pd 3d$_{3/2}$ peak (eV)	ΔPd 3d$_{5/2}$ (eV)
Pd NPs	335.0	340.2	0
TOH Au@Pd$_{1L}$ NPs	335.1	340.3	0.1

Table S5. XPS shifts of the Au 4f signals of TOH Au NPs and TOH Au@Pd$_{1L}$ NPs prepared in aqueous CTAC solution with a pH of 3.3.

Sample	Au 4f$_{7/2}$ peak (eV)	Au 4f$_{5/2}$ peak (eV)	ΔAu 4f$_{7/2}$ (eV)
TOH Au NPs	83.8	87.5	0
TOH Au@Pd$_{1L}$ NPs	83.7	87.4	-0.1

Table S6. Summarized data of ECSA values, mass activities, and specific activities of the corresponding TOH Au@Pd NPs, cubic Au@Pd NPs, spherical Au@Pd NPs, and commercial Pd/C catalysts. The differently-shaped Au@Pd$_{island}$ NPs and Au@Pd$_{1L}$ NPs were prepared in the aqueous CTAC solution with a pH of 7.5 and 3.3, respectively.

Sample	ECSA [m^2 g$_{Pd}^{-1}$]	Mass activity [A mg$_{Pd}^{-1}$]	Specific activity [mA cm^{-2}]
TOH Au@Pd$_{island}$ NPs	49.6	4.9	8.2
TOH Au@Pd$_{1L}$ NPs	100.9	13.2	13.1
cubic Au@Pd$_{island}$ NPs	41.2	2.6	6.3
cubic Au@Pd$_{1L}$ NPs	84.9	9.0	10.6
spherical Au@Pd$_{island}$ NPs	64.3	4.1	6.4
spherical Au@Pd$_{1L}$ NPs	90.7	8.6	9.4
commercial Pd/C catalysts	31.0	0.2	0.6

31

Table S7. The ordinary Raman shifts of 4-NTP and 4-ATP, and their assignments.

	SERS (cm^{-1})	Assignment
4-NTP	854	C-H wagging
4-NTP	1080	C-S stretching
4-NTP	1108	O-N-O stretching
4-NTP	1336	O-N-O stretching
4-NTP	1572	phenyl-ring mode
4-ATP	1078	C-S stretching
4-ATP	1173	C-H in plane bending
4-ATP	1592	phenyl-ring mode

References

(1) A. Habrioux, W. Vogel, M. Guinel, L. Guetaz, K. Servat, B. Kokoh, N. Alonso-Vante, *Phys. Chem. Chem. Phys.,* 2009, 11, 3573–3579.

(2) C. Bi, C. Feng, T. Miao, Y. Song, D. Wang and H. Xia, *Nanoscale*, 2015, **7**, 20105–20116.